Solid-State Supramolecular Organization of Polythiophene Chains Containing Thienothiophene Units

By *Patrick Brocorens,* Antoine Van Vooren, Michael L. Chabinyc, Michael F. Toney, Maxim Shkunov, Martin Heeney, Iain McCulloch, Jérôme Cornil,* and *Roberto Lazzaroni*

We use molecular modeling and the simulation of X-ray diffraction patterns to determine the molecular packing of a thiophene-based polymer showing exceptionally high field-effect mobilities (up to 1 $cm^2 V^{-1} s^{-1}$). We focus on the organization of the polymer chains in lamellae and the orientation of these crystalline domains with respect to the substrate in thin films. The analysis is supported by XRD and NEXAFS experiments and is complemented by calculating intermolecular transfer integrals, which govern the charge mobility.

1. Introduction

Conjugated polymers are widely investigated for organic electronics as they can be processed at low cost over large areas and yield mechanically flexible devices. When used as active semiconducting layers in organic field-effect transistors (FETs), thiophene-based polymers have demonstrated carrier mobilities ranging from 0.1 to 1 $cm^2 V^{-1} s^{-1}$ (i.e., values high enough for many applications[1–4]) that are intimately linked to their supramolecular organization in the solid state. Solution-processible semiconducting polymers such as regioregular poly(3-hexylthiophene) (P3HT) are made of a conjugated backbone along which alkyl groups are grafted to improve solubility. During film formation, these two components self-segregate, often giving rise to a lamellar structure with stacks of conjugated backbones separated by layers of alkyl groups. The lamellae can orient differently—parallel or normal—to the substrate, dramatically changing the mobility in the plane of the film (by more than a factor of 100 for P3HT).[1] Such a high anisotropy reflects an interchain transport of the charge carriers that is much more efficient along the π-stacking direction and along the backbones than through the layers of packed alkyl groups. The mobility is thus maximized when the π-stacking direction or the long chain axes is aligned along the flow of current, i.e., when the lamellae are parallel to the substrate.

Recently, poly(2,5-bis(3-alkylthiophen-2-yl)thieno[3,2-b]thiophene) (PBTTT) has been reported to have improved stability to air and

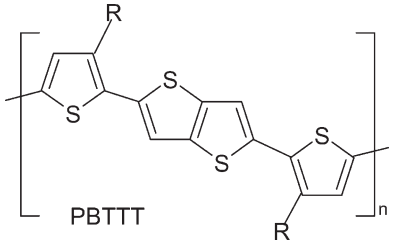

light, and higher mobilities (up to 0.6 $cm^2 V^{-1} s^{-1}$ in long channel and 1 $cm^2 V^{-1} s^{-1}$ in short channel FETs) relative to P3HT.[2,4] This high charge carrier mobility is achieved by thermally annealing cast films into a liquid-crystalline mesophase and then by cooling back to room temperature. The annealing improves the structural ordering in the films, as evidenced by X-ray scattering and atomic force microscopy measurements: large lateral terraces extending over several hundreds of nanometers are observed.[2,5] Additionally, since the specific volume difference between crystalline and liquid-crystalline phases is small, the polymer segments located between the crystalline domains are probably less disordered upon crystal growth, thus potentially

[*] Dr. P. Brocorens, A. Van Vooren, Dr. J. Cornil, Prof. R. Lazzaroni
Laboratory for Chemistry of Novel Materials,
University of Mons-Hainaut
Place du Parc, 20, Mons 7000 (Belgium)
E-mail: patrick@averell.umh.ac.be
Prof. M. L. Chabinyc
Materials Department, University of California
Santa Barbara, CA 93106-5050 (USA)
Dr. M. F. Toney
Stanford Synchrotron Radiation Laboratory
Menlo Park, CA 94025 (USA)
Dr. M. Shkunov
Advanced Technology Institute, University of Surrey
Guildford, Surrey GU2 7XH (UK)
Dr. M. Heeney
Department of Materials, Queen Mary, University of London
Mile End Road, London E1 4NS (UK)
Prof. I. McCulloch
Imperial College London, South Kensington Campus
London SW7 2AZ (UK)

DOI: 10.1002/adma.200801668

reducing charge trapping.[6] Calculations of the transport properties carried out on model stacks of PBTTT and P3HT oligomers indicate that the mobility is hardly affected by the nature of the repeat unit but is extremely sensitive to the relative position of the chains.[7] Thus, the improvement in carrier mobility is related to several factors including the size, orientation, and ordering of the crystalline domains, as well as the molecular packing of the chains and the nature of structural defects.

Understanding how charge transport properties are influenced by the supramolecular organization of the molecules is of paramount importance to design new molecular structures or new device architectures aiming at higher device efficiencies. So far, most of the theoretical studies of charge transport have relied on model lattices or are limited to probe the evolution of the properties when changing the relative orientation of the molecules, due to the lack of structural data (except for molecular crystals). There are only few detailed packing structures known for semiconducting polymers. Significant effort has been made to determine experimentally and to model the ordering of poly(alkylthiophenes). In most of these studies, X-ray scattering data are recorded and modeled,[1,8–13] but the materials show relatively few diffraction peaks, making the modeling task challenging so that uncertainties about the structures generally remain. In contrast, PBTTT is a highly favorable material for setting up and validating a joint theoretical and experimental methodology for studying the organization of semiconducting polymers in films since uncertainties about the structure are significantly reduced due to the unprecedently high crystallinity and orientation of the chains. Simulations of the molecular packing, X-ray diffraction (XRD) patterns, and charge transport properties are combined here to determine the molecular packing in PBTTT lamellae, the orientation of these crystalline domains with respect to the substrate and the resulting electronic coupling between the chains. The validity of our approach has been assessed by direct comparison to XRD and near edge X-ray absorption fine structure (NEXAFS) measurements (experimental details are reported elsewhere).

2. Results

The systems considered here are thin films (70–100 nm) of PBTTT substituted by dodecyl groups (PBTTT-C12), which were spin-coated on silicon oxide surfaces modified by octyltrichlorosilane, followed by annealing at 180 °C. Both the PBTTT synthesis and formation of films were described previously.[2,14] The structure of the crystalline domains of the films was inferred by simulation techniques, following a procedure in four steps to funnel the research toward the equilibrium structure:

(i) The torsion potentials around the bonds connecting the thiophene units of the PBTTT backbone were first evaluated to determine whether the backbone adopts a planar conformation upon packing of the molecules. This information is necessary as the next step consists in modeling the PBTTT chain conformation in crystalline domains from a conformational search performed on isolated molecules, i.e., where packing effects are absent. In PBTTT chains, two-third of the junctions between the thiophene and/or thienothiophene subunits are head-to-tail (HT), and one-third are tail-to-tail (TT). Data in the literature[15,16] and our B3LYP and PBE/6-31G** density functional theory (DFT) calculations show that both junctions can planarize easily upon packing because this conformational change induces little intrachain energetic penalty and allows larger interchain interactions. As a result, the junctions in PBTTT were set planar.

(ii) A conformational search was performed with a force field technique on a long isolated oligomer. A lamellar organization of the polymers implies that backbone layers and alkyl layers alternate, with a dense packing expected in both types of layers. Few conformations of a polymer chain are compatible with such an organization, thus requiring the use of both geometry and energy criteria to select the best candidates. Six PBTTT conformers were generated, all having alkyl groups that are out-of-plane with respect to the conjugated backbone. The most stable conformer corresponds to an all-*anti* conjugated backbone and has the best geometrical characteristics: the backbone is straight (with bent backbones, helical or disordered structures occur), and the alkyl groups are oriented in the same direction (in the solid state, this structure favors a dense packing in the alkyl layer via tilting, interdigitation, and nesting). Other conformers are less stable, due to *syn* junctions, and have snaky or helical backbones, with alkyl groups pointing in different directions. In conclusion, from both the geometry and energy point of view, the conformer expected in well-organized assemblies has an all-*anti* configuration.

(iii) A crystal cell was built containing one monomer unit (i.e., the substituted thiophen-2-ylthieno[3,2-b]thiophene motif repeated along the backbone direction). The monomer unit was linked to its images in the neighboring cells to produce an all-*anti* polymer chain. The initial parameters of the cell were adjusted to reproduce an infinite stack of infinite polymer chains, with either interdigitated (I) or non-interdigitated (NI) alkyl side groups; those systems were optimized with a force field technique (see structural properties in Table 1). The two polymorphs are characterized by small

Table 1. Structural properties of the simulated crystal cells of PBTTT described in the text; the cells' parameters set fixed during the optimization process are indicated in bold.

PBTTT-C12	NI	I	IM26	IT35
Backbone tilt angle [a]	4°	10°	7°	18°
Alkyl tilt angle [a]	68°	43°	40°	28°
Lamella thickness (Å)	18.7	17.2	19.5	19.1
Density	1.22	1.28	1.06	1.09
Along stacking [b]	3.5	3.5	3.8	3.6
Lateral [b]	−0.2	0.8	0.3	1.2
Longitudinal [b]	−6.3	−3.6	−3.6	−3.9
Cell Parameters a (Å)	20.7	17.4	**19.5**	**19.6**
b (Å)	7.2	5.0	**5.2**	**5.4**
c (Å)	13.5	13.6	13.5	**13.6**
α	151.3°	135.0°	**133.0°**	**136.0°**
β	114.7°	92.6°	**90.0°**	**84.0°**
γ	71.1°	82.4°	**90.0°**	**86.0°**

[a] [a] Tilt angle of the conjugated backbones and alkyl groups with respect to the normal to the substrate. [b] Displacements (Å) between the backbones of adjacent chains in the π-stacks.

lateral displacements (0.2–0.8 Å) and short (3.5 Å) spacing between adjacent backbones in the same layer, which is typical for dense packing of π-stacking molecules. The cross-sectional area of the alkyl groups (i.e., the area occupied by the alkyl groups when viewed along the alkyl group direction) is ~18 Å^2, similar to the experimental limiting cross-sectional area of alkane molecules[17] (18 Å^2) and to the value (17 Å^2) found for optimally stacked alkane molecules studied with the same force field. The very good packing of the alkyl groups in both polymorphs is related to their aptitude to tilt and orient differently with respect to the backbone so as to maintain an optimal density in the crystal. This explains why the density does not change much from NI to I (1.2 vs. 1.3). As a result, the interlayer spacing does not change much either (18.7 Å vs. 17.2 Å). Despite these similarities, NI differs substantially from I in terms of the relative longitudinal displacement of adjacent backbones in the π-stack (6.3 Å for NI vs. 3.6 Å for I). Non-interdigitated systems are expected to have larger longitudinal displacements of the molecules and larger tilting of the alkyl groups than interdigitated systems, as it is a way to fill voids that are occupied by alkyl groups from the neighboring layer in the interdigitated configurations. However, the van der Waals stabilization energy of NI is smaller than that of I since the tilt of the alkyl groups does not increase sufficiently the density. Moreover, deformations of the alkyl skeleton occur, thus leading to a sharp increase of the energy terms related to bonds, angles, and torsions (by 4.1 kcal mol^{-1} monomer unit^{-1}). As a result, NI is much less stable than I, by 14.7 kcal mol^{-1} monomer unit^{-1}. PBTTT is therefore expected to be interdigitated.

(iv) To further confirm that PBTTT is interdigitated, the 2D XRD patterns of I and NI were simulated and compared to experimental patterns (Fig. 1) reported previously.[14] The data are expressed as a function of the scattering vector, q (the d-spacing of a peak is $2\pi/q$). In the 2D patterns, the q component that is orthogonal to the sample surface is displayed along the vertical axis (q_z) while the component parallel to the sample surface is displayed along the horizontal axis (q_{xy}), in order to get information about the orientation of the molecules in the film. The PBTTT films are highly textured. The domains are preferentially oriented with the a^* axis (axis orthogonal to the lamellae plane) along q_z, but in the film plane they are randomly oriented. As a result, in plane, it is not important to distinguish q_x from q_y, and only q_{xy} is considered. The simulation results for NI do not match the experimental data, missing the row of weak spots at $q_{xy} \sim 0.7$ Å^{-1}, and showing a row of intense spots at $q_{xy} \sim 1.0$ Å^{-1} instead of ~1.4 Å^{-1}. The pattern of I fits much better the experiment, confirming that PBTTT is interdigitated. Still, some discrepancies exist. They are attributed to small differences between the simulated and real cells due to approximations in the simulation methods used to reproduce the intermolecular interactions. The cell parameters have thus to be refined to give a better match between the experimental and simulated patterns. To do so, an indexation of selected experimental spots was proposed from the simulated pattern; the positions of these spots were then calculated varying systematically the six cell parameters, and were compared to the experimental positions using an RMS deviation criterion. Sets of parameters corresponding to the smallest RMS were applied to crystal cells, which were then optimized with these new cell parameters set fixed. The 2D patterns were finally simulated and compared to experiment. All generated cells are interdigitated

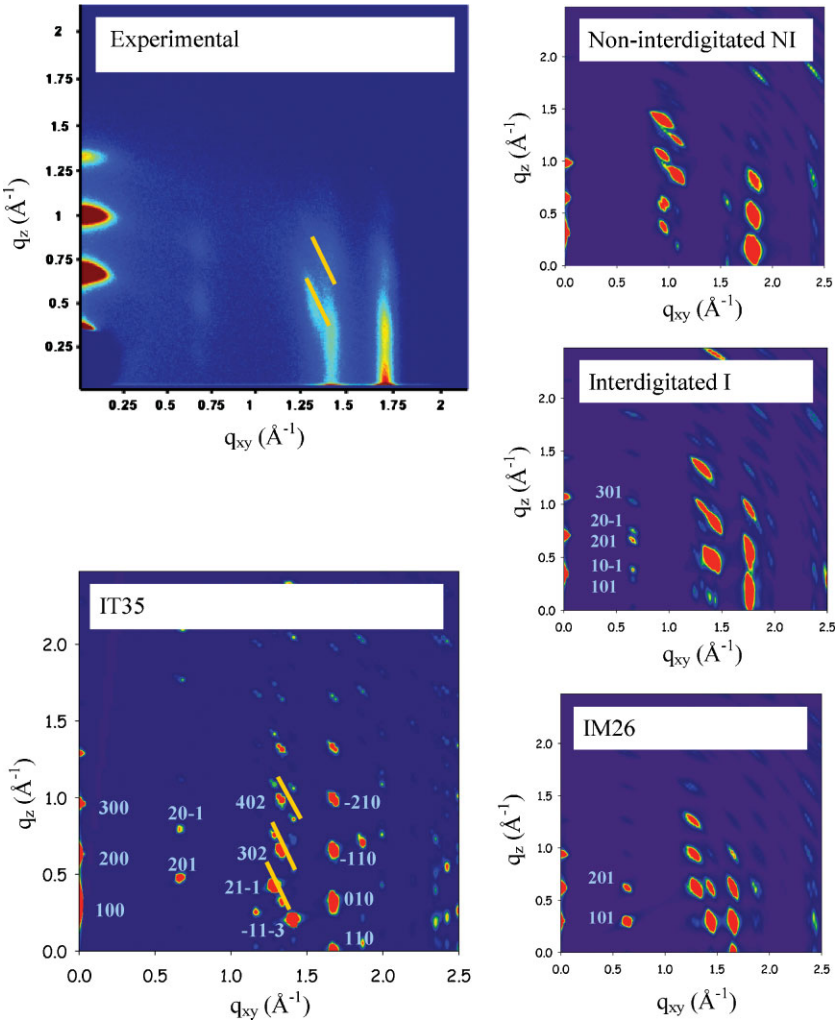

Figure 1. Experimental and simulated 2D XRD patterns of PBTTT for the non-interdigitated configuration NI, and interdigitated configurations I, IM26, IT35. For I, NI, and IM26, a low level of disorder of the crystallites in the film (with a standard deviation $\sigma = 2°$) and a small peak broadening (0.2°) are considered. For IT35, smaller standard deviation ($\sigma = 0.75°$) and peak broadening (0.1°) are used to better localize the individual diffraction peaks.

and triclinic (IT). In order to confirm that the PBTTT crystals are triclinic instead of monoclinic or orthorhombic as it has been suggested,[2] several interdigitated monoclinic (IM) cells were also considered. The numbers following T or M hereafter correspond to the numbering of the systems in the list of polymorphs that were evaluated.

A common characteristic of the monoclinic (and orthorhombic) cells is that the spots along q_z at $q_{xy} \sim 0.0$ and $0.7\,\text{Å}^{-1}$ corresponding to (h00) and (h01) planes, respectively, have the same q_z in the simulation (see IM26 in Fig. 1), because the (h00) and (001) planes are orthogonal. Since this positioning is not observed experimentally, we can conclude that the cell is triclinic. In triclinic cells, the (h00) planes can be non-orthogonal to the (001) planes, leading to a splitting of the (h01) planes into (h01) and (h0–1) planes with $q_z \sim q_z$ (h00) $\pm\, q_z$ (001), as observed in I for the spots along q_z at $q_{xy} \sim 0.7\,\text{Å}^{-1}$. The number of spots is twice that observed experimentally, but for particular combinations of cell angles, q_z (001) $\sim$ ½ q_z (100), and spots of different k form doublets and appear at the same q_z. This specific case is observed for IT35, contributing to make IT35 the PBTTT structure that best fits the experimental data (see Supplementary Information). There is thus a wealth of information that can be extracted from the 2D experimental spectra to tune the simulated cell.

The indexing of the IT35 diffraction pattern is here described by analyzing the rows of spots along q_z. The (100) peak corresponding to the lamellar spacing (19.1 Å) appears at $q_{xy} \sim 0.0\,\text{Å}^{-1}$ with a very intense progression of higher order (h00) peaks, whose declining intensity matches the experimental observation. The (001) peak corresponding to the planes delimiting a monomer unit along the backbone direction is at $q_{xy} \sim 0.7\,\text{Å}^{-1}$, but it is not observed due to its very weak intensity. The (k10) peaks appear at $q_{xy} \sim 1.7\,\text{Å}^{-1}$. As the cell is triclinic, the most intense peak at $q_z \sim 0\,\text{Å}^{-1}$ is the (110) plane. The (010) plane, expected to be parallel to the backbone plane, appears at $q_z \sim 0.37\,\text{Å}^{-1}$, indicating that the backbone is tilted with respect to the substrate. Based on the experimental q_{xy} and q_z, the tilt angle of the (010) plane is estimated to be about 12°, and the spacing is 3.6 Å. A similar result is obtained on the basis of IT35, but it appears that the conjugated backbone does not lie perfectly in the (010) plane, thus increasing the tilt angle of the backbone with respect to the substrate to 18° (Fig. 2), while still maintaining the interbackbone spacing at 3.6 Å. The tilt angle of the backbone is similar to that (21°) found for PBTTT-C14 using NEXAFS spectroscopy and DFT calculations.[18] The analysis of the peaks at $q_{xy} \sim 1.7\,\text{Å}^{-1}$ also reveals that the (110) spot is not located exactly at $q_z = 0\,\text{Å}^{-1}$. Hence, the spots at $q_{xy} = 1.7\,\text{Å}^{-1}$ are actually composed of doublets of spots very close to one another. For instance, the spot attributed to (010) is actually composed of two spots, (010) and (210), displaced along q_z by $0.06\,\text{Å}^{-1}$. This assignment could also explain why in the experimental pattern these peaks appear broadened along q_z, instead of perpendicularly to the scattering vector, as occurs usually when the crystallites are misoriented. Arced broadening is also visible in the pattern, for peaks at $q_{xy} = 1.3\,\text{Å}^{-1}$ (as highlighted by the oblique lines in the experimental pattern of Fig. 1). Instead of misorientation, this observation could be due to the fact that the most intense peaks are accompanied by less intense peaks in a direction that is perpendicular to the scattering vector (see IT35 Fig. 1).

The peaks at $q_{xy} = 1.3$ and $1.4\,\text{Å}^{-1}$ have a high sensitivity, both in position and in intensity, to the orientation of the alkyl groups. They are thus also strongly sensitive to small variations of the cell parameters (as seen for instance in Fig. 1 when comparing those peaks in I, IM26, and IT35), while those at $q_{xy} = 1.7\,\text{Å}^{-1}$ are far less sensitive. The sensitivity to the orientation of the alkyl groups materializes into strong variations of the tilt angles of the alkyl groups with respect to the normal to the film in the different cells (see

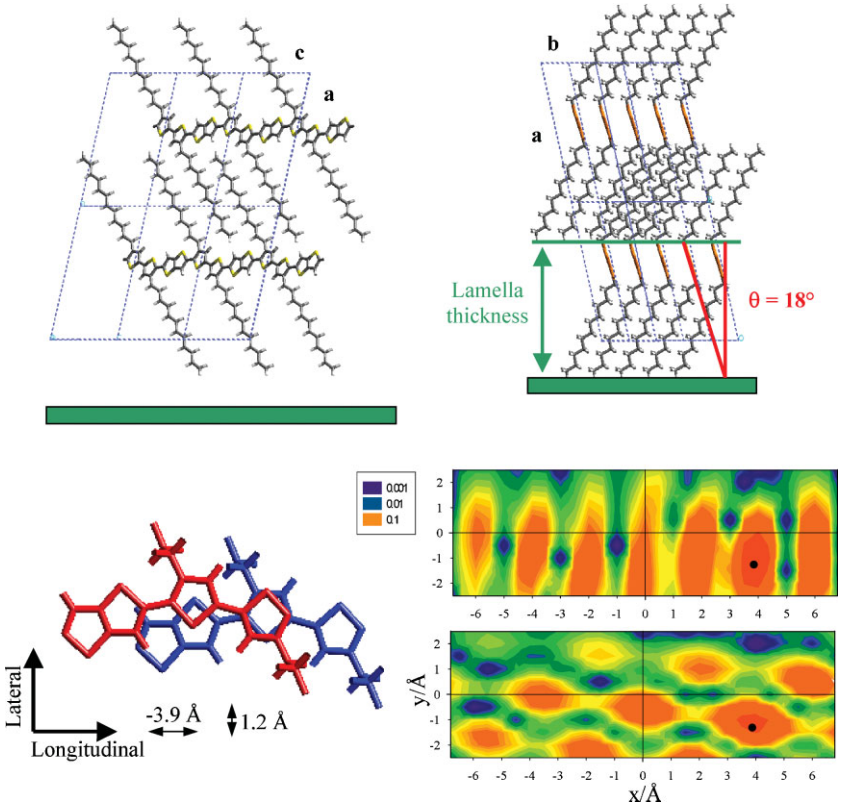

Figure 2. Top: IT35 polymorph of PBTTT viewed along *b* (left) and *c* (right); the crystallite is represented in its preferential orientation with respect to the substrate; the tilt angle of the backbone with respect to the substrate normal is 18°. Bottom left: Monomer units of adjacent chains in IT35, viewed orthogonally to the backbone planes and with their relative displacements indicated. Bottom right: ZINDO-calculated transfer integrals *t* (in eV) between HOMOs (top) and LUMOs (bottom) for two adjacent PBTTT dimers separated by an intermolecular distance of 3.6 Å. The transfer integrals have been calculated for the IT35 geometry (in 0,0) and for different relative positions of the oligomers obtained by sliding one oligomer laterally (*y*-axis) and longitudinally (*x*-axis); the dot represents the position of the perfectly cofacial dimer.

Table 1). In IT35, the alkyl groups are tilted by ~28°. NEXAFS data on PBTTT-C14 also showed that the alkyl groups are significantly tilted, by about 45° for that system.[18] Despite large variations in the simulated patterns for rows of spots at $q_{xy} = 1.4$ Å^{-1}, there are only very weak peaks in the equatorial plane, and the most intense peak, attributed to (-11-3), has a non-zero q_z contribution. This prediction has been confirmed experimentally by recording a slice at $q_{xy} = 1.4$ Å^{-1}.[19]

Finally, the relationship between the supramolecular organization and the charge transport properties was analyzed by computing the transfer integrals t between chain segments. The transfer integrals reflect the strength of the electronic interactions between adjacent molecules and govern the charge mobility in the band and hopping regimes; they were calculated at the semiempirical Hartree–Fock intermediate neglect of differential overlap (INDO) level in a dimer made of two adjacent PBTTT oligomers containing two monomer units, according to a method previously described.[7] The initial relative position and structure of the oligomers were extracted from IT35. In order to assess the influence of deviations from that packing geometry on charge transport, t was also calculated for different relative positions of the oligomers, as obtained by sliding one oligomer laterally and longitudinally by steps of 0.5 Å, with the intermolecular distance fixed at 3.6 Å. The evolution of t for the HOMO (hole transport) and LUMO (electron transport) levels is illustrated in Figure 2. The transfer integrals are among the highest for the IT35 structure (i.e., the 0,0 coordinate in Fig. 2) both for holes and electrons. This result further supports our analysis that IT35 is close to the PBTTT equilibrium packing geometry, since it is consistent with the high mobility values measured for PBTTT, and points to the ambipolar transport properties of the material (provided that the charge injection is optimized for both carriers, as observed recently for other polymers).[20] Note that the transfer integrals can drop by at least one order of magnitude upon small relative displacements (less than 1 Å) of the chains, thus suggesting that the conformational dynamics of the chains might affect transport properties.

3. Conclusions

The film organization of PBTTT shown in Figure 2 is consistent with all available data: the calculated structure and charge transport properties, the XRD experiments and simulations, and the NEXAFS experiments reported for a similar PBTTT system. In this structure, the molecules are interdigitated and form lamellae parallel to the substrate. The backbone planes, as well as the alkyl groups, are tilted with respect to a normal to the substrate. The excellent hole transport properties reported for the material are explained by a combination of favorable factors: the longitudinal and lateral relative displacements of the backbones (by ~3.9 and 1.2 Å, respectively) preserve large transfer integrals, the distance between the conjugated backbones is short (3.6 Å), the molecules are well ordered and well oriented on the substrate, and the crystalline domains are large. Furthermore, this work demonstrates the validity of the simulation methodology developed here and opens the way to study other semiconducting polymers in highly ordered thin films.

4. Simulation Details

4.1. Force Field Calculations

The conformational search was performed with Cerius2 [21] on tetramers, which were optimized by molecular mechanics using the UFF [22,23] force field slightly modified to better reproduce the thiophene geometry and maintaining the backbone planar. Atomic charges were assigned by the PCFF force field [24-26]. The geometry optimizations were performed with the Conjugate Gradient method with an RMS force criterion of 0.001 kcal mol^{-1} Å^{-1}. The long-range non-bonded interactions were turned off using the Spline method, with spline-on and spline-off parameters set to 11 and 14 Å, respectively. The crystal structures were optimized by a similar procedure, using periodic boundary conditions and turning off the long-range non-bonded interactions by the Ewald method. The Ewald parameters were optimized to reach an energy accuracy of 10^{-4} kcal mol^{-1}.

4.2. X-Ray Scattering Simulations

We used the method explained below for simulating out-of-plane patterns (this can be generalized to simulate 2D patterns). In a film of oriented crystallites, one crystal plane is preferentially oriented parallel to the substrate. This plane, called the *reference plane*, is the plane contributing to out-of-plane diffraction for oriented crystallites. For misoriented crystallites, the *reference plane* gives no signal, and instead, others planes are parallel to the substrate and give a signal. In crystallites deviating by φ degrees from the preferential orientation, the crystal planes giving a signal are those deviating by φ degrees from the *reference plane*. The population distribution of the crystallites as a function of the deviation (represented by a Gaussian function whose standard deviation σ can be varied to reproduce different degrees of disorder in the film), was then used to ponder the intensity I_{n0} of each diffraction peak at $2\theta_n$ and simulated for an isotropic sample by Cerius2. [21]

$$I_n = I_{n0} \frac{1}{\sigma\sqrt{2\pi}} e^{\left(\frac{-\varphi^2}{2\sigma^2}\right)}$$

An instrumental broadening of the peaks I_n was then given by a Lorentzian function independent of 2θ, in such a way that the intensity I of the pattern at 2θ is

$$I = \sum_n \frac{1}{\frac{(2\theta - 2\theta_n)^2}{\Delta^2}} I_n$$

The broadening is adjusted by the parameter Δ (to match the experimental peak width).

Acknowledgements

This work was supported by the European Union NAIMO Integrated Project (NMP4-CT-2004-500355), the Interuniversity Attraction Pole program of the Belgian Federal Science Policy Office (PAI 6/27), and by FNRS-FRFC. J. C. is an FNRS Research Associate; A. V. V. acknowledges a grant from Fonds pour la Formation à la Recherche dans l'Industrie et dans l'Agriculture (FRIA). Portions of this research were carried out at the Stanford Synchrotron Radiation Laboratory, a national user facility operated

by Stanford University on behalf of the U.S. Department of Energy, Office of Basic Energy Sciences. Supporting Information is available online from Wiley InterScience or from the author.

Published online: February 11, 2009

[1] H. Sirringhaus, P. J. Brown, R. H. Friend, M. M. Nielsen, K. Bechgaard, B. M. W. Langeveld-Voss, A. J. H. Spiering, R. A. J. Janssen, E. W. Meijer, P. Herwig, D. M. de Leeuw, *Nature* **1999**, *401*, 685.
[2] I. McCulloch, M. Heeney, C. Bailey, K. Genevicius, I. MacDonald, M. Shkunov, D. Sparrowe, S. Tierney, R. Wagner, W. Zhang, M. L. Chabinyc, R. J. Kline, M. D. McGehee, M. F. Toney, *Nat. Mater.* **2006**, *5*, 328.
[3] B. S. Ong, Y. Wu, P. Liu, S. Gardner, *J. Am. Chem. Soc.* **2004**, *126*, 3378.
[4] B. H. Hamadani, D. J. Gundlach, I. McCulloch, M. Heeney, *Appl. Phys. Lett.* **2007**, *91*, 243512.
[5] R. J. Kline, D. M. DeLongchamp, D. A. Fischer, E. K. Lin, M. Heeney, I. McCulloch, M. F. Toney, *Appl. Phys. Lett.* **2007**, *90*, 062117.
[6] A. Salleo, T. W. Chen, A. R. Völkel, Y. Wu, P. Liu, B. S. Ong, R. A. Street, *Phys. Rev. B* **2004**, *70*, 115311.
[7] B. M. Milián, A. Van Vooren, P. Brocorens, J. Gierschner, M. Shkunov, M. Heeney, I. McCulloch, R. Lazzaroni, J. Cornil, *Chem. Mater.* **2007**, *19*, 4949.
[8] T. J. Prosa, M. J. Winokur, J. Moulton, P. Smith, A. J. Heeger, *Macromolecules* **1992**, *25*, 4364.
[9] R. J. Kline, M. D. McGehee, E. N. Kadnikova, J. Liu, J. M. J. Fréchet, M. F. Toney, *Macromolecules* **2005**, *38*, 3312.
[10] S. Joshi, S. Grigorian, U. Pietsch, *Phys. Stat. Sol.* **2008**, *205*, 488.
[11] R. D. McCullough, S. Tristram-Nagle, S. P. Williams, R. D. Lowe, M. Jayaraman, *J. Am. Chem. Soc.* **1993**, *115*, 4910.
[12] K. Tashiro, M. Kobayashi, *Polymer* **1997**, *38*, 2867.
[13] S. A. Chen, S. J. Lee, *Polymer* **1995**, *36*, 1719.
[14] M. L. Chabinyc, M. F. Toney, R. J. Kline, I. McCulloch, M. Heeney, *J. Am. Chem. Soc.* **2007**, *129*, 3226.
[15] M. Takayanagi, T. Gejo, I. Hanozaki, *J. Phys. Chem. A* **1994**, *98*, 12893.
[16] J. C. Sancho-García, J. Cornil, *J. Chem. Phys.* **2004**, *121*, 3096.
[17] D. K. Schwartz, *Surf. Sci. Rep.* **1997**, *27*, 241.
[18] D. M. DeLongchamp, R. J. Kline, E. K. Lin, D. A. Fischer, L. J. Richter, L. A. Lucas, M. Heeney, I. McCulloch, J. E. Northrup, *Adv. Mater.* **2007**, *19*, 833.
[19] Private Communication with M. L. Chabinyc.
[20] J. Cornil, J. L. Bredas, J. Zaumseil, H. Sirringhaus, *Adv. Mater.* **2007**, *19*, 1791.
[21] Accelrys, formerly Molecular Simulation Inc, 9685 Scranton Road, San Diego, CA; **1997**.
[22] C. J. Casewit, K. S. Colwell, A. K. Rappé, *J. Am. Chem. Soc.* **1992**, *114*, 10035.
[23] A. K. Rappé, C. J. Casewit, K. S. Colwell, W. A. Goddard, III, W. M. Skiff, *J. Am. Chem. Soc.* **1992**, *114*, 10024.
[24] H. Sun, *J. Comp. Chem.* **1994**, *15*, 752.
[25] H. Sun, S. J. Mumby, J. R. Maple, A. T. Hagler, *J. Am. Chem. Soc.* **1994**, *116*, 2978.
[26] H. Sun, S. J. Mumby, J. R. Maple, A. T. Hagler, *J. Phys. Chem.* **1995**, *99*, 5873.